

**Original citation:**

Ebejer, Neil, Güell, Aleix G., Lai, Stanley C. S., McKelvey, Kim, Snowden, Michael E. and Unwin, Patrick R.. (2013) Scanning electrochemical cell microscopy : a versatile technique for nanoscale electrochemistry and functional imaging. Annual Review of Analytical Chemistry, Volume 6 (Number 1). p. 130411102155005. ISSN 1936-1327

Permanent WRAP url:

<http://wrap.warwick.ac.uk/54234/>

Copyright and reuse:

The Warwick Research Archive Portal (WRAP) makes the work of researchers of the University of Warwick available open access under the following conditions. Copyright © and all moral rights to the version of the paper presented here belong to the individual author(s) and/or other copyright owners. To the extent reasonable and practicable the material made available in WRAP has been checked for eligibility before being made available.

Copies of full items can be used for personal research or study, educational, or not-for-profit purposes without prior permission or charge. Provided that the authors, title and full bibliographic details are credited, a hyperlink and/or URL is given for the original metadata page and the content is not changed in any way.

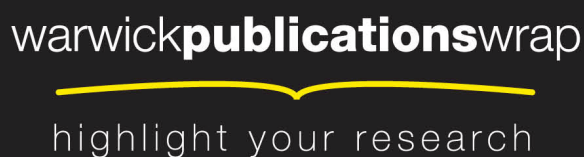
Publisher's statement:

Posted with permission from the Annual Review of Analytical Chemistry, Volume 6 (Number 1) © by Annual Reviews, <http://www.annualreviews.org>

A note on versions:

The version presented here is a working paper or pre-print that may be later published elsewhere. If a published version is known of, the above WRAP url will contain details on finding it.

For more information, please contact the WRAP Team at: wrap@warwick.ac.uk



<http://go.warwick.ac.uk/lib-publications>

EBEJER ET AL.

ELECTROCHEMICAL IMAGING

SCANNING ELECTROCHEMICAL CELL MICROSCOPY: A Versatile Technique for Nanoscale Electrochemistry and Functional Imaging

Neil Ebejer,¹ Aleix G. Güell,¹ Stanley C.S. Lai,¹ Kim McKelvey,^{1,2} Michael E. Snowden,¹ and Patrick R. Unwin¹

¹*Department of Chemistry, and ²MOAC Doctoral Training Center, University of Warwick, Coventry CV4 7AL, United Kingdom; email: P.R.Unwin@warwick.ac.uk*

■ **Abstract** Scanning electrochemical cell microscopy (SECCM) is a new pipette-based imaging technique purposely designed to allow simultaneous electrochemical, conductance, and topographical visualization of surfaces and interfaces. SECCM uses a tiny meniscus or droplet, confined between the probe and the surface, for high-resolution functional imaging and nanoscale electrochemical measurements. Here we introduce this technique and provide an overview of its principles, instrumentation, and theory. We discuss the power of SECCM in resolving complex structure-activity problems and provide considerable new information on electrode processes by referring to key example systems, including graphene, graphite, carbon nanotubes, nanoparticles, and conducting diamond. The many longstanding questions that SECCM has been able to answer during its short existence demonstrate its potential to become a major technique in electrochemistry and interfacial science.

Keywords scanning probe microscopy, electrocatalysis, carbon nanotubes, graphene, nanoparticles, micropipettes and nanopipettes

1. INTRODUCTION

Since its introduction in 2010, scanning electrochemical cell microscopy (SECCM) (1) has developed into a versatile scanning probe microscopy technique suitable for many applications. The probe in SECCM is a double-barreled (theta) pipette, filled with

electrolyte solution, together with contacting quasi-reference counterelectrodes (QRCEs) in each channel. A thin meniscus droplet at the end of the pipette constitutes a mobile, nanoscopic electrochemical cell that can be brought into contact with a surface for high-resolution electrochemical (ion-transfer and electron-transfer) imaging, with positional feedback and the possibility of elucidating topographical features. The technique is amenable to high-level quantitative analysis, and owing to the experimental design, high mass-transfer rates are readily achieved, allowing for the study of fast kinetic processes. In this review, we outline the fundamental basis of SECCM and some of its key applications. We begin by placing the development of SECCM in context by referring to earlier pipette-based imaging methods, micro- and nanofluidic devices, and electrochemical imaging in general. We conclude by highlighting potential future prospects and discuss the ongoing advances of the technique.

SECCM is a recent addition to a large family of scanning electrochemical probe microscopy methods. Among these techniques, scanning electrochemical microscopy (SECM), originally developed in the late 1980s (2, 3), is one of the best known. Its operation is based on the use of an ultramicroelectrode placed closed to, and scanned across, a surface to quantitatively probe interfacial physicochemical processes (4--8). Many papers have been published on SECM, and this technique and its applications have been extensively reviewed (5, 9--11). Although powerful as a means of resolving surface phenomena, SECM has drawbacks that limit the materials and processes that can be studied. First, in (conventional) SECM there is no mechanism to maintain a constant tip-to-substrate separation. Consequently, this requires samples to be flat and precisely aligned and has limited SECM mainly to the use of disk-shaped tips with diameters of 1 to 25 μm . Various efforts have been made to incorporate positional feedback into SECM to overcome this issue and enhance the spatial resolution (9, 12--24). Second, SECM requires the entire sample to be immersed in electrolyte solution and held at conditions wherein it is active for the time it takes to perform the experiments (up to hours), which may lead to changes in surface properties of both the sample and the tip. Finally, SECM is a remote sensing technique that relies on the diffusion of species between the sample surface and the tip.

Although solid electrodes are the main type of probe in SECM, pipette-based probes have also been implemented, particularly for facilitated (25) and simple (26) ion transfer

across liquid/liquid interfaces. In this case, the pipette contains an electrolyte (e.g., organic solution) that is immiscible with the solution into which it is placed (e.g., aqueous solution), and the system operates in a similar manner to traditional SECM (6). Its applications include electrochemical imaging of electrode surfaces (5), local delivery of species to a substrate surface, and metal deposition (27).

Soft stylus--type probes have also been developed to facilitate imaging of very large samples compared with those usually studied in SECM (28, 29). Due to the flexibility of these probes, which are pushed into contact with the substrate of interest, they can track topographical features without the need for complex electronic feedback circuits. A further enhancement is the use of arrays of these probes to reduce the experimental timescale (28). By inserting a microfluidic channel, with an integrated counter/reference electrode, into this type of probe, investigators have fabricated a fountain pen--like probe to allow the characterization of dry surfaces (30). Although it is an interesting innovation within scanning droplet-based techniques, this system is designed to have a large footprint to study extended areas of a sample.

Pipette-based electrochemical methods, which use a liquid meniscus formed at the end of the pipette, were originally developed for high-resolution corrosion studies, in which it was necessary to confine measurements to a small area of surface. In its original form, the setup utilized a single-channel pipette probe with a diameter between 100 and 1,000 μm , with the end coated in a thick silicone rubber gasket to prevent evaporation and to define the electrode area (31, 32). The pipette was mounted on a microscope, allowing easy positioning on the surface, with the gasket at the end forming a tight seal. This setup allowed for the electrochemical interrogation of localized pitting sites on stainless steel (31, 32). An automated probe-positioning system was also attempted; in this system the substrate was mounted onto piezoelectric actuators and oscillated at the resonant frequency, with either a damping of the oscillation amplitude or a shift in the resonant frequency used to detect probe landing (33). To incorporate the possibility of moving the scanning droplet cell across the surface, a liquid droplet was used that was not confined by a gasket (34--36).

Investigators subsequently developed a flow-through microcell reactor to collect products of reactions carried out at large current densities for off-line analysis of reactions (37). These authors used a dual-channel (theta) capillary with a footprint of several hundred micrometers across, defined by a silicone gasket. Electrolyte flow was

achieved via an external pump, and this approach has been used mostly for metal electrodisolution/corrosion studies (38--40).

The scanning micropipette contact method (41) uses a mobile micropipette (dimensions between hundreds of nanometers to tens of micrometers) to conduct high-resolution electrochemical measurements. The technique operates in air (or another controlled environment), and the pipette is filled with an electroactive species in electrolyte solution, with a QRCE inserted. The probe is translated toward the surface with a bias applied between the QRCE and the working electrode, which has to be a (semi)conducting substrate, to carry out a redox reaction of the electroactive species inside the pipette. Once the liquid meniscus at the end of the probe makes contact with the surface, an electrochemical current is detected and the motion of the probe is halted to ensure that the probe itself does not make physical contact. Various local electrochemical measurements can then be made. The probe is then retracted and moved to a new position (in air) parallel to the surface, and a new approach is made. The electrochemical activity of the surface can be thus built up on a point-by-point basis, although the process is relatively slow. This technique has been used to demonstrate the electrochemical activity of the basal plane of highly oriented pyrolytic graphite (HOPG) and to study the corrosion activity of aluminum alloys (41). A simpler version of this technique, the microcapillary electrochemical method, allows microscopic cells to be readily made with small portions of complex substrates (42, 43).

In parallel with the droplet-based techniques highlighted above and SECM, scanning ion conductance microscopy (SICM) was introduced in the late 1980s, purely as a noncontact topographical imaging technique (44). The system operates by generating an ion current between a QRCE in a sharp micro- or nanopipette and a second QRCE in the bathing solution. Probe positioning is achieved through a feedback mechanism based on a hindered ion flow between the two QRCEs, which occurs once the pipette probe comes into close proximity with a surface. Initially, the feedback mechanism was based on the mean conductance current between the QRCEs (44), but this mechanism proved to be rather unstable because it was sensitive to local changes in ionic strength and blockage of the electrode. Not until a decade later was positioning improved through the use a modulated ion current generated by a physical oscillation of the probe, perpendicular to the surface (45, 46). More recently, a multiple-approach curve methodology at an array of points over the surface was employed to study topographically challenging samples, such as neurons (47). Most SICM applications have been for topographical imaging of

live cells, although ion-transfer measurements have also been attempted more recently (46), and SICM can also be used for patch clamping (48, 49). The combination of SICM and SECM (50--52) also adds chemically specific flux mapping capabilities to SICM topographical imaging.

The use of a modulated ion current due to probe oscillation has also been implemented for the patterning of surfaces with biomolecules from a theta pipette (53). The authors of this study used a double-barreled micro- or nanopipette that contained a QRCE in each barrel and was filled with an aqueous electrolyte solution. An ion current flowed through a liquid meniscus at the end of the pipette, and once surface contact was made, a modulation in the ion current was established due to a modulation in resistance (53, 54). This technique was operated either in air or under an immiscible organic solution.

SECCM builds on the double-barreled micro- or nanopipette idea by combining it with simultaneous electrochemical measurements, primarily electron transfer at a substrate but also ion transfer. Furthermore, SECCM exploits the possibility of controlling the bias potential between the QRCEs to control mass transport. As we highlight herein, this innovation surpasses other droplet systems previously developed for electrochemical imaging and opens up many new possibilities for nanoscale electrochemistry and functional mapping. SECCM has already allowed us to perform studies and acquire information about electrochemical interfaces that was previously impossible or extremely challenging to obtain, and is revealing many new insights, as described below.

2. SCANNING ELECTROCHEMICAL CELL MICROSCOPY SETUP AND INSTRUMENTATION

2.1. Instrumentation

Figure 1a shows the present configuration for SECCM. This setup is used to investigate the surface of interest, and when that surface is a (semi)conductor, a working electrode is formed whose area is defined by the contact area of the meniscus at the end of the pipette with the surface. A potential (V_2) is applied between the QRCEs in the barrels to induce an ionic conductance current, i_{dc} , across the liquid meniscus. This bias is typically kept constant during the course of an experiment to maintain a constant ionic current across the liquid meniscus at the end of the pipette. The potential of the QRCEs can be floated (V_1) with respect to ground while maintaining the constant bias potential

between the two QRCEs. By adjusting V_1 while holding V_2 fixed, the the relative potential of a (semi)conducting substrate can be controlled with respect to the QRCEs. Moreover, the current at (semi)conducting substrates can be measured as i_{WE} . The effective potential of the substrate with respect to the QRCEs is approximately $-(V_1 + V_2/2)$ because the barrels of the pipette are typically symmetrical with the septum in the center of the pipette, and both barrels are the same size. The probe should be kept vertical with respect to the surface and the two QRCEs should be identical (55). This assignment of the effective potential of the substrate is further borne out in the measured reversible half-wave potentials for well-known redox couples that are consistent between SECCM and conventional voltammetry.

<COMP: PLEASE INSERT FIGURE 1 HERE>

Figure 1 (a) Schematic of the scanning electrochemical cell microscopy (SECCM) setup. A quasi-reference counter electrode is immersed in each barrel of a theta pipette probe, which is filled with the solution of interest. Piezoelectric positioners are employed for pipette z-modulation and displacement toward the sample, and for lateral scanning. (b) Field emission scanning--electron microscopy (FE-SEM) images of a double-barreled pipette used as the probe in SECCM, and FE-SEM images of imprints left from SECCM landings on amorphous carbon films, prove that the contact area is comparable to the probe dimensions. (c) SECCM approach curves of dc conductance current and the ac component are a function of z-piezoelectric extension toward the substrate. Three regions are identified: in air, when the meniscus has not yet established contact with the substrate; jump-to-contact; and contact.

Movement of the pipette is controlled by three piezoelectric positioners. Our group has described two instrument configurations that differ in how the lateral (x - y) movement of the pipette is achieved (1, 56). The first system employs a tip-scanning configuration in which the probe is mounted on a stack of three (x - y - z) piezoelectric positioners, which allows the probe to be moved in three dimensions while the sample is held stationary. The second system is a sample scanning configuration in which the probe is mounted on a single (z) piezoelectric positioner, which allows movement normal to the surface, while the sample is mounted on two (x - y) piezoelectric positioners that allow lateral movement. For most applications, and particularly for high-resolution imaging, the sample scanning configuration is preferred because it reduces possible cross talk between the piezoelectric positioners. However, this configuration does require the sample to be mounted on the piezoelectric positioners, and large mass and strain on the positioners should be avoided. Additionally, a voltage-wave generator, either external or built into a lock-in amplifier (software or hardware based) is used to

oscillate the probe, sinusoidally, normal to the surface and to extract the induced ac component of the ionic conductance (barrel) current (i_{ac}), which is used as a feedback signal to control the distance between the end of the probe and the surface. The piezoelectric positioners, potential control of the QRCEs, and current amplifiers are typically monitored and controlled through a data-acquisition or field-programmable gate array card that is, in turn, controlled from a computer running custom software (typically written in LabVIEW from National Instruments).

2.2. Probes

SECCM employs pulled (borosilicate or quartz) theta pipettes as probes. The spatial resolution depends on the size of the pulled theta pipette (**Figure 1b**), which can be fabricated to the desired dimensions (~100 nm to tens of micrometers, depending on the application) by use of a laser puller. Hitherto, the overwhelming majority of SECCM studies have employed aqueous electrolyte solutions. Therefore, after the pipette is pulled, the outer wall is usually silanized with dimethyldichlorosilane [$\text{Si}(\text{CH}_3)_2\text{Cl}_2$], rendering it hydrophobic, which helps to confine the aqueous meniscus to the very end of the tip (57). Both barrels are then filled with an electrolyte solution and, if desired, a redox mediator of interest. A QRCE, typically an Ag/AgCl electrode (1, 55, 56, 58, 59) or a Pd-H₂ electrode (60, 61), is inserted into each barrel.

Finally, the local wetting properties of the substrate must be taken into account. Although the contact area is determined mostly by the size of the pipette, which provides a good rule of thumb for the spatial resolution, the contact radius may vary by up to 10-20% of the pipette radius for particularly hydrophilic [such as (oxygen-terminated) polycrystalline boron--doped diamond (pBDD)] or hydrophobic (such as HOPG) substrates. In such cases, the contact area can be accurately determined by deposition experiments.

2.3. Working Principles

A potential bias is applied between the QRCEs in the barrels to induce an ion conductance current (i_{dc}) across the liquid meniscus formed at the end of the pipette, and changes in this conductance current are used as a feedback signal to position the probe at a set distance from the surface. Specifically, the probe is modulated, sinusoidally, normal to the surface, and once contact between the liquid meniscus and the surface is established, the ion current across the meniscus shows a periodic modulation at the same frequency of oscillation due to the reversible deformation of the meniscus. The

magnitude of the ac component (i_{ac}) of the conductance current is detected through the use of lock-in techniques and used as a feedback parameter for controlling the tip-to-substrate separation. Typical oscillation frequencies and peak-to-peak amplitudes are approximately 70-300 Hz and 20-100 nm, respectively. **Figure 1c** shows typical responses of both i_{dc} and i_{ac} as a probe (1 μm in diameter, filled with 50 mM of KCl solution, using Ag/AgCl QRCEs) is carefully moved toward a surface (HOPG) at a constant speed (50 nm s^{-1}). Initially, the meniscus is not in contact with the surface, and the dc conductance current is constant, with a negligible ac component. At the point that contact is made between the meniscus and the surface, a large jump in i_{dc} is observed due to the sudden deformation of the meniscus (jump to contact with the surface), and i_{ac} increases accordingly by several orders of magnitude for the reasons given above. As the probe is moved closer to the surface (at 2 nm s^{-1}), the meniscus is squashed between the probe and the surface, resulting in a decrease in i_{dc} but an increase in i_{ac} , due to the increasing gradient of i_{dc} with distance as probe height decreases. . Also, as highlighted above, in cases in which the substrate is (semi)conducting, one can make direct electrochemical measurements in which the contacted area between the meniscus and the substrate constitutes the working electrode (**Figure 1b**).

2.4. Scan Procedure

Once the meniscus is brought into contact with the surface, it is moved laterally while a constant tip-to-substrate separation is maintained (thereby ensuring meniscus contact with the surface); the probe height is adjusted to maintain constant i_{ac} . Two methods for updating the height of the probe, based on a user-defined i_{ac} set point, can be employed: a distance-based method and a time-based method. In the distance-based method, once the probe has moved a user-defined lateral distance, which is set depending on the pipette size, roughness of the sample, and desired spatial resolution, the ac magnitude is measured and the height of the pipette is updated on the basis of the difference between the ac magnitude and the set point. Then, the probe may pause, for a user-defined time, to record the substrate and conductance currents. This pattern is repeated as the probe is moved laterally across the sample. In the time-based method, the probe is moved laterally over the surface at a constant velocity and the height of the probe is simultaneously updated at set time intervals (typically on the millisecond scale, which is effectively continuous for the velocities used). Current signals are measured continuously as the probe is moved laterally across the surface. This method provides a

much higher spatial resolution of current measurement and reduces the time needed to record an image, making it the preferred method for most applications. The increased spatial resolution is particularly advantageous when using small-size tips and when the sample has small features. Our group now uses this approach exclusively.

Two-dimensional images of the electrochemical activity of a surface are typically constructed from a series of parallel line scans. During each line scan, the probe is moved forward over a line and then often reversed over the same line before being moved to the next line. Thus, from a single scan, two sets (one from forward lines and one from reverse lines) of maps can be constructed for the surface current (working electrode activity), the dc ion conductance current, the magnitude of the ac component of the conductance current, and surface topography (from the height of the probe) as function of lateral pipette position. **Figure 2** shows these sets of data for a HOPG sample (56). Note that in addition to the ac magnitude, the phase can also be measured, although we have not considered the phase in detail in SECCM studies.

<COMP: PLEASE INSERT FIGURE 2 HERE>

Figure 2 Set of maps acquired simultaneously during scanning electrochemical cell microscopy scans of highly oriented pyrolytic graphite for the reduction of $\text{Ru}(\text{NH}_3)_6^{3+}$ at the reversible half-wave potential. Both forward (*left*) and reverse (*right*) scans are shown. (a) The working electrode response. (b) The ionic dc conductance current (i_{dc}) between the barrels in the pipette. (c) The ac component of the ion current (i_{ac}) used as a feedback parameter. (d) A topographical map from the z -piezoelectric displacement. Adapted with permission from Reference 56. Copyright 2012, Wiley-VCH.

The surface current map identifies local changes in surface activity and is of primary interest when investigating the electroactivity of surfaces. Surface kinetic measurements can be obtained from this map with the use of appropriate modeling techniques (55, 58, 59). The dc conductance current map is often relatively featureless during the mapping of electrode substrates, although it can be a sensitive way to identify variations in the size of the meniscus, for example, due to changes in local wetting properties; in **Figure 2b**, the meniscus moves across the hydrophobic HOPG surface and intermittently encounters hydrophilic (monolayer and bilayer) step edges. Moreover, changes in the ionic composition of the meniscus during the scan, for instance, from the dissolution of the substrate or by local ion uptake at the substrate, can be identified from the dc conductance current map (1).

The ac conductance magnitude is used as the feedback parameter to keep a set distance between the probe and the surface, and as such, this map is typically flat.

However, as in atomic force microscopy (AFM), this error signal map can help identify certain features, such as the edges in the HOPG surface in **Figure 2c**. Finally, the probe height as a function of probe lateral position is used to generate a two-dimensional map of the apparent surface topography, and remarkable resolution is evident (e.g., **Figure 2d**), particularly given that a droplet employed for imaging is typically several hundreds of nanometers in diameter. For the different maps described above, comparisons between the forward and reverse line scans allow for the identification and validation of features and enable identification of any changes in the surface activity (e.g., due to fouling).

3. MODELING AND SIMULATION OF SCANNING ELECTROCHEMICAL CELL MICROSCOPY

3.1. Simulation Overview

A quantitative description of mass transport is crucial for understanding and interpreting SECCM experimental data. A finite-element method (FEM) model describes the main features of mass transport in SECCM (55), which we briefly highlight here. **Figure 3a** shows the geometry used for the SECCM probe, meniscus, and substrate (defined herein as the working electrode). The theta pipette is approximated to a capped, truncated cone, where the cap represents the opening, and the meniscus is typically represented with a cylinder; variations of this geometry have been explored in some detail (55). The key geometrical parameters to consider in describing the ion conductance across the meniscus between the QRCEs, and mass transport to the substrate, are the internal radius of the pipette (r_p), the semiangle (θ), the thickness of the central septum (t_w), and the tip-to-substrate separation (or, equivalently, the meniscus height m_h) and the effective bias in the simulated domain (E_f). Experimentally, r_p , θ , and t_w can be measured accurately using field emission scanning electron microscopy (FE-SEM); the height of the meniscus is derived from the experimental data with the aid of simulation (see Section 3.2) (55, 58, 59)

<COMP: PLEASE INSERT FIGURE 3 HERE>

Figure 3 (a) Schematic of the scanning electrochemical cell microscopy (SECCM) assembly showing the simulated domain and critical parameters. (b) Simulated potential field for a pipette with $r_p = 0.5 \mu\text{m}$, $\theta = 7^\circ$, $m_h = 0.4 \mu\text{m}$, and $E_f = 0.5 \text{ V}$. (c) Comparison between the i_{dc} and i_{ac} experimental and simulated approach curves for a pipette with $r_p = 0.5 \mu\text{m}$ and $\theta = 7^\circ$ that is filled with 50 mM of KCl and oscillated at an amplitude of 50 nm. (d) Experimental cyclic voltammetry scans for the oxidation of 2

mM of FcTMA⁺ (ferrocenylmethyl) trimethylammonium) in 50 mM of KCl, within an SECCM probe with $r_p = 0.6 \mu\text{m}$, $m_h = 0.15 \mu\text{m}$, and $\theta = 8.5^\circ$, for potential differences between the barrels of 0, 0.1, 0.2, 0.3, 0.4, and 0.5 V. (e) Comparison between the response of the limiting current, $i_{\text{WE lim}}$, for experimental data (*circles*) and data from simulations (*stars*) for the probe used in panel d. Adapted with permission from Reference 55. Copyright 2012, American Chemical Society.

3.2. Potential Field

Mass transport within the SECCM probe is due primarily to migration and diffusion of chemical species, which can be elucidated by solving the Nernst--Planck equation:

$$\frac{\partial c_j}{\partial t} + \nabla(-D_j \nabla c_j - z_j u_j F c_j \nabla V) + \mathbf{u} \nabla c_j = R_j. \quad (1)$$

Here, c_j is the concentration, D_j is the diffusion coefficient, z_j is the charge, R_j is the rate of any homogeneous reaction within the domain, u_j is the ionic mobility of species j , t is time, V is the electric field, and \mathbf{u} is the velocity vector of the solution within the pipette. We assume that \mathbf{u} is zero because the contribution due to electro-osmosis (62--64) is negligible compared with those from diffusion and migration for the experimental conditions employed so far, as determined by the Smoluchowski equation (65). Figure 3b shows the potential field for a pipette with $r_p = 0.5 \mu\text{m}$, $\theta = 7^\circ$, and $m_h = 0.4 \mu\text{m}$ that is filled with 50 mM of KCl, where K⁺ ions have a mobility of $u_{\text{K}^+} = 7.3 \times 10^{-8} \text{ m}^2 \text{ s}^{-1} \text{ V}^{-1}$ and Cl⁻ ions have a mobility of $u_{\text{Cl}^-} = 7.6 \times 10^{-8} \text{ m}^2 \text{ s}^{-1} \text{ V}^{-1}$ at $T = 298 \text{ K}$ (66). A potential field of 0.5 V was set between planes p_1 and p_2 . The gradient of the potential field is steepest in the areas of highest resistance, near the tip of the pipette, and within the meniscus. When there is no reaction within the pipette or at the surface, the ion conductance is directly proportional to the potential bias between the barrels (55).

The tip-to-substrate separation in SECCM can readily be determined by analysis of the ac and dc components of the ion conductance current as a function of distance when the meniscus is in contact with the substrate. As the tip-to-substrate separation decreases initially, i_{dc} decreases but i_{ac} increases. The increase in i_{ac} is the result of the increasing gradient of i_{dc} with decreasing height. There is excellent agreement between the experimental and simulated approach curves for the example of a pipette with $r_p = 0.5 \mu\text{m}$ and $\theta = 7^\circ$ that was filled with 50 mM of KCl and oscillated at an amplitude of 50 nm (70 Hz) (Figure 3c). Furthermore, the height of the pipette above the surface can evidently be set and deduced by monitoring both i_{ac} and i_{dc} .

3.3. Electrochemical Reaction at the Substrate Working Electrode

As discussed above, data from simulations of the voltammetric response of the working electrode in SECCM agree with data from experiments (55). Figure 3d shows typical SECCM cyclic voltammetry data for a probe with $r_p = 0.6 \mu\text{m}$, $m_h = 0.15 \mu\text{m}$, and $\theta = 8.5^\circ$ that was filled with 2 mM of (ferrocenylmethyl) trimethylammonium (FcTMA^+) as the hexafluorophosphate salt in 50 mM of KCl; FcTMA^+ underwent a one-electron oxidation as the potential of the substrate was swept from 0.0 V to 0.65 V versus Ag/AgCl. The data illustrate that increasing the potential difference between the QRCEs in the barrels of the pipette (V_2 in Figure 1a), with values of 0, 0.1, 0.2, 0.3, 0.4, and 0.5 V (Figure 3d), increases the working electrode limiting current because of the increasing contribution to mass transport from migration. Figure 3e further shows that the steady-state experimental limiting current can be simulated to a high level of accuracy (55).

In practice, two approaches can simulate reactions at the substrate working electrode surface, carefully balancing a trade-off between accuracy and computational resources: the dynamic field and static field approaches. In the dynamic field approach, the electric field that controls the migration of ions between the barrels of the pipette is recalculated for the changing conductivity within the SECCM probe arising from the working electrode reaction. In the static field approach, the potential field is calculated for the initial conditions (with no reaction occurring at the substrate) and kept constant when a substrate reaction is introduced. In other words, the electric field is assumed not to be significantly perturbed by the substrate reaction. The latter approximation is less computationally demanding and provides a reasonable approximation for cases in which the substrate reaction has a negligible impact on the conductivity of the solution within the meniscus, that is, where there is a large concentration of supporting electrolyte with respect to the redox-active species. The dynamic field is used for cases in which the conductivity is significantly affected by the substrate reaction, such as (a) when the supporting electrolyte concentration is similar to that of the redox-active species and (b) when the local solution conductivity in the meniscus and at the end of the pipette is likely to change significantly (typically by more than 5%).

4. ILLUSTRATIVE EXAMPLES OF SCANNING ELECTROCHEMICAL CELL MICROSCOPY

4.1. Novel Carbon (Electrode) Materials

A major focus of SECCM has been carbon materials, which are of great interest for many electrochemical applications because of their exceptional electronic and optical properties (67), chemical and mechanical stability, and ease of functionalization (68). There are different allotropes of carbon depending on the atomic hybridization, yielding large variations in the intrinsic properties. For example, diamond is intrinsically an insulator (69), whereas graphene is a semimetal; it exhibits the highest electron mobilities ever reported (70). Furthermore, different macroscopic arrangements of certain carbon materials are also possible; such arrangements range from aligned single-walled nanotube (SWNT) wires to three-dimensional SWNT forests and from single- to multilayer graphene. Certain configurations enhance material-specific electrochemical properties (58, 71, 72), but unless the fundamental nature of heterogeneous electron transfer is understood, it is difficult to optimize these devices. SECCM has allowed us to study and understand these materials by using micro- and nanosized mobile electrochemical cells that can isolate the different components of each material of interest; this technique requires little preparation, encapsulation, or lithography of the sample, which might otherwise influence the response. Moreover, SECCM images can be correlated with information from complementary analytical and microscopy techniques to provide a comprehensive view of structure and reactivity.

4.2. Point Measurements: From Voltammetry to Local Capacitance

A major advantage of SECCM is that the position of the pipette can be controlled precisely to confine electrochemical measurements to a single point on a surface of (sub)micrometer dimensions. This capability is particularly powerful for samples on which the features are irregularly shaped or spaced, or would otherwise prove difficult to prepare or encapsulate in the form of micro- and nanoscale electrodes with conventional lithographic techniques. The latter aspect is particularly important as surface contamination associated with some lithographic processing may pose a problem (73). In contrast, SECCM provides a different route to assembling nanoscale electrochemical cells: A small droplet is simply brought to a desired location on a surface of interest. Although such measurements can, in principle, also be performed with single-barreled pipettes, the use of a theta pipette offers an extra degree of control over the mass transport of charged species (Figure 2d,e) and allows estimation of the meniscus height (Figure 2c).

As an exemplar system, point measurements have been made on pBDD (61, 74), which is a heterogeneous electrode material due to variations in boron uptake by different facets during pBDD growth that cause variations in local dopant concentration (75). Such variations in dopant concentration, as well as the possible presence of sp^2 carbon contamination (especially at grain boundaries), have led to considerable debate on the active sites for electron transfer (ET) on pBDD (75--78). Using SECCM, we have made microscale voltammetric measurements on regions of the surface with varying boron concentrations; the results indicated a very strong effect of the local substrate properties on the electron-transfer kinetics for the simple inner-sphere redox mediator $Fe^{2+/3+}$ (61). SECCM has also been employed, as part of a multimicroscopy approach, to perform localized capacitance measurements on various pBDD facets to link electrochemical reaction rates with the local boron concentration (74). In this study, variations in localized electron-transfer rates were visualized with intermittent contact (IC)-SECM (21) and were quantified by FEM modeling. Local boron concentrations were determined using FE-SEM and micro-Raman spectroscopy measurements. To measure local capacitance values with SECCM, the authors took care to minimize stray capacitance, allowing the measurement of capacitance values in facets with different characteristic boron concentrations at micrometer-sized contact areas. From these capacitance values, the local density of electronic states was found to correlate with the local reaction kinetics, indicating that variations in localized reactivity are associated with variations in dopant concentration (74).

Because of its ability to confine electrochemical measurements on complex substrates, SECCM has been used to study the electrochemical activity of vertically aligned (SWNT) forests (79). In this application, SECCM allowed the experimenters to access the ends and the sidewalls of the nanotubes independently; the forest was in its pristine form, and no photolithography or encapsulation was needed. To verify that the contact area was similar for measurements at the ends and the sidewalls, the authors measured the ion current between the two barrels of the SECCM probe, which is a reasonable indicator of meniscus size for the experimental conditions employed. This study highlighted that the nanotube sidewalls are highly electrochemically active for outer-sphere redox complexes such as $Ru(NH_3)_6^{3+/2+}$ and $FcTMA^{+/2+}$, and that comparable electrochemical activity is found at SWNT end sites. Furthermore, the results showed that SWNT ensembles can be used as electrodes in their pristine form

and that postprocessing to open SWNT ends is unnecessary for the redox reactions considered.

Finally, we have also exploited the ability of SECCM to form a nanoscopic electrochemical cell to perform nanoparticle landing experiments (92). The probe was filled with a colloidal solution of gold nanoparticles (AuNPs) in an electrolyte solution, and the meniscus was brought into contact with a ‘collector’ electrode. The collector electrode was held at a potential where an electrocatalytic reaction occurred on the AuNP but not on the collector electrode. Consequently, the arrival of AuNPs at the electrode surface resulted in a stepwise increase in the current at the collector electrode, and each current step could be assigned to the (cumulative) response of a single nanoparticle. Because electrodes with small areas are required to limit the number of nanoparticle landings and to minimize the background current on the collector electrode, such experiments are typically performed using an ultramicroelectrode immersed in an electrolyte solution (93,94,95) as a collector electrode. In our approach, rather than decreasing the area of the collector electrode through the manufacture of an ultramicroelectrode, we employed SECCM to limit the area in contact with the solution (92). This has a number of advantages. First, the electrode area is smaller than that of a typical UME, resulting in lower background currents, which allowed us to measure smaller currents from the nanoparticle reaction. Second, it allows the use of a wide range of materials for the collector electrode, including materials which cannot be shaped into an ultramicroelectrode. Finally, we are able to make and break the cell at will, for example after the landing of a predetermined number of particles. Using this SECCM-based approach, we were able to detect the landing of AuNPs on HOPG (which is particularly advantageous because of its low background current) at a potential where dissolved oxygen is reduced on the AuNP, even though the current step per AuNP was less than 1 pA. Furthermore, we were able to land a single NP on a carbon coated transmission electron microscope (TEM) grid and correlate its electrochemical reactivity with the structural properties obtained with TEM, thereby enabling structure-activity relationships to be studied at the level of a single nanoparticle.

4.3. Mapping and Visualizing Heterogeneous Electron Transfer at the Nanoscale

SECCM is at its most powerful when used to scan across the substrate of interest to produce x - y maps of surface reactivity, simultaneously with topography and ion conductance. This technique is particularly useful for elucidating variations in reactivity

as a function of the properties of the substrate electrode. We have employed SECCM to map the electrochemical reactivity of several carbon materials for which there has been controversy on the nature of the active sites for electron transfer (**Figure 4**). For example, as discussed above, pBDD is inherently heterogeneous due to variations in dopant density across the different facets. Electron transfer on a pBDD surface might be dominated by the grain boundaries or other hot spots (76). **Figure 4** shows an example of a SECCM reactivity map of pBDD for the oxidation of the neurotransmitter serotonin (5-hydroxytryptamine), a complex multistage reaction (61). This map clearly shows patterns of electrochemical activity that strongly correspond to the local dopant density obtained with FE-SEM. In addition, no enhanced current was observed at grain boundaries or at other hot spots. Similar results were found for the outer-sphere couple $\text{FcTMA}^{+/2+}$ and the ‘simple’ inner-sphere couple $\text{Fe}^{2+/3+}$ (61).

Importantly, the reactivity mapping of serotonin oxidation illustrates that SECCM can be employed to study reactions in which the product blocks the electrode surface because the reaction is notorious for electrode fouling (72, 80--82). Although electrode fouling was still observed in the SECCM study, the reaction product was left behind during imaging when the tip was moved to a new position and a reactivity map was readily obtained, demonstrating the strength and versatility of SECCM as an imaging technique.

<COMP: PLEASE INSERT FIGURE 4 HERE>

Figure 4 Summary of a wide range of applications of scanning electrochemical cell microscopy (SECCM). Single-point measurement for voltammetry (55). Electrochemical interrogation of nanosized structures such as nanoparticles (adapted with permission from Reference(60). Copyright 2011, American Chemical Society.) and nanotubes (adapted with permission from Reference (59). Copyright 2012, National Society of Sciences of the United States of America.) Investigation of heterogeneous electrode materials with examples of exfoliated graphene, highly oriented pyrolytic graphite, (adapted with permission from Reference (56). Copyright 2012, Wiley-VCH.) and polycrystalline boron--doped diamond (pBDD) (adapted with permission from Reference (61). Copyright 2012, American Chemical Society.) Abbreviations: AFM, atomic force microscopy; FE-SEM, field emission scanning--electron microscopy.

Within the family of carbon materials, sp^2 carbon--based materials such as graphene and carbon nanotubes are attracting particular attention. Different types of graphene, such as mechanically exfoliated graphene and chemical vapor deposition (CVD) grown graphene have been interrogated with SECCM (**Figures 4, 5**). Among them, graphene grown by CVD methods on nickel substrates consists of a heterogeneous, continuous layer of single-layered and multi-layered micrometer-sized graphene flakes (83) and is

ideal for demonstrating the capabilities of SECCM as an electrochemical mapping technique. The random orientation, shape, and distribution of these flakes make their individual interrogation incompatible with other techniques. For SECCM studies, the size of the double-barreled pipettes employed was fine-tuned, according to the average size of the flakes, to ensure single-flake interrogation and to minimize the contributions from surrounding flakes. **Figure 5** compares a typical electrochemical map for the one-electron oxidation of the outer-sphere mediator FcTMA^+ obtained via SECCM with images from complementary techniques, such as AFM, optical microscopy, and micro-Raman (58). Investigators usually consider three primary Raman peaks to assess the number of layers, doping, functionalization, lattice defects, and physical damage of graphene (84). The Raman spectra for four different flakes confirmed that darker regions on the optical microscopy images corresponded to thicker graphene flakes. These data sets revealed a very strong correlation between the electrochemical activity of graphene and the number of graphene layers; multi-layered flakes exhibited the highest electrochemical activity. These findings have important implications for the design and optimization of new graphene-based technology, particularly for electrochemical applications.

<COMP: PLEASE INSERT FIGURE 5 HERE>

Figure 5 Characterization of the same region of chemical vapor deposition—grown – graphene on an Si/SiO₂ substrate with (a) scanning electrochemical cell microscopy substrate-current map, (b) optical microscopy, and (c) atomic force microscope topography. There is a striking correlation between structure and activity. (d) Complementary micro-Raman (633-nm laser) single-point measurements of four regions (inset) to determine graphene structural characterization in greater detail. Adapted with permission from Reference 58. Copyright 2012, American Chemical Society.

HOPG is interesting both in its own right and as a comparative case for graphene studies, given that it comprises an infinite number of stacked graphene layers. By studying the HOPG basal surface, with a step spacing significantly larger than the pipette diameter, researchers investigated the HOPG basal plane electrochemically, in isolation from the response on the step edges, for the first time (56)(96,97). **Figure 2** shows SECCM maps for the one-electron reduction of $\text{Ru}(\text{NH}_3)_6^{3+}$ at the reversible half-wave potential. The surface current maps (**Figure 2a**) show that the entire surface is electrochemically active. The HOPG basal plane supports fast electron transfer (close to reversible) for two commonly used redox probes, $\text{Ru}(\text{NH}_3)_6^{3+/2+}$ and $\text{Fe}(\text{CN})_6^{4-/3-}$, even under the high mass-transport rates delivered by the SECCM setup (see Section 3.3). In

contrast, a previous model derived from conventional macroscopic measurements considered the basal surface to be completely or largely inert (85). Thus, SECCM is valuable in being able to test such models for surface activity directly. Reasons for the difference between SECCM studies and earlier work have been assessed and discussed fully (96).

4.4. Intrinsic Electrochemical Properties of Nanomaterials

A further advantage of SECCM is that the feedback mechanism for the tip-to-sample separation does not rely on the electrical nature of the substrate, enabling one to image substrates that are (partially) insulating. This advantage allowed the study of two-dimensional networks of SWNTs grown by CVD on silicon/silicon oxide, which constituted only 0.3% of the otherwise nonelectrochemically active surface. In this case, the theta pipettes were employed (~250 nm) that were smaller than the typical spacing between nanotubes (59), which allowed the acquisition of maps of electrochemical activity with high spatial resolution and to extract information from individual nanotubes. The electrochemical activity of the SWNTs was studied through outer-sphere redox couples, such as $\text{FcTMA}^{+/2+}$ and $\text{Ru}(\text{NH}_3)_6^{3+/2+}$. The resulting electrochemical maps (Figures 4, 6) revealed that the nanotubes had substantial activity. This finding, in addition to the lack of current enhancement or hot spots across the surface (for example, at nanotube ends), suggests a new model for SWNT electrochemical activity in which the sidewalls should be considered active components.

<COMP: PLEASE INSERT FIGURE 6 HERE>

Figure 6 (a) Scanning electrochemical cell microscopy (SECCM) image (working electrode response) of a two-dimensional single-walled nanotube (SWNT) network on Si/SiO₂, highlighting an individual line scan. (b) The motion of the SECCM nanoprobe across a single SWNT, resulting in a peak profile. Also shown are scenarios in which one or three defects are present on a sidewall that is otherwise inert. (c) Experimental data for an individual SWNT peak profile during a line scan compared with simulated data from the case of a fully active sidewall; there is activity at only one point defect or three point defects. Adapted with permission from Reference 59. Copyright 2012, National Society of Sciences of the United States of America.

To further confirm this finding and eliminate the possibility that only defect points in the sidewalls are responsible for heterogeneous electron transfer at SWNTs, the investigators analyzed scan profiles across individual nanotubes, highlighting a further powerful feature of SECCM for kinetic mapping (59). As the SECCM meniscus scans from the inert SiO₂ surface over a nanotube (perpendicular to the scan direction), a

gradual increase (and then decrease) in the working electrode current is measured because of a gradual increase (and then decrease) in the area of the nanotube being contacted by the droplet. This behavior arises from small incremental portions of nanotube that are more or less equally electrochemically active when accessed at each step (typically 5 nm) in the scan. FEM model simulations were used to validate these results, and scan profiles were simulated for a fully active SWNT, together with one- and three-point defects in the accessed area on an otherwise inactive SWNT; these values are reasonable estimates of the typical defect density and maximum defect density on this type of SWNT (86). For the cases in which only point-defects were considered to be electrochemically active, the experimentally measured current could not be match by the currents obtained from FEM simulations (Figure 6), even when unrealistically high standard electron transfer rate constants ($k^0 > 10^3 \text{ cm s}^{-1}$) were assigned to the point defects. Thus, SECCM line profiles are very powerful in distinguishing between different models for characteristic activities in nanoscale materials, that would be difficult to achieve with conventional techniques. The ability to use SECCM on (partially) non-electrochemically active substrates was further exploited to study the reactivity of discreet individual platinum nanoparticles (PtNPs) (60). PtNPs of ~100-nm size were electrodeposited on an isolated SWNT, which acted as a wire to electrically connect the PtNP; the interparticle spacing was in the micrometer range. SECCM was used to locate and investigate the potential-dependent reactivity of individual PtNPs. Figure 4 shows a typical image. These particles were subsequently characterized with AFM and FE-SEM, enabling a direct correlation between the reactivity of the PtNP and its size and shape. The results showed that subtle variations in nanoparticle morphology can lead to dramatic changes in the (potential-dependent) activity, which has important implications for the design and optimization of nanoparticles in electrochemical applications. Also, the SECCM setup can be employed to study events with very low currents (down to ~10 fA over a 40 ms period, which corresponds to only ~2,500 electron-transfer events). This study demonstrated SECCM's major potential for investigations of electrode reactions at the single-nanoparticle level by drawing on the technique's excellent spatial and current resolution. Such studies could help investigators gain a true fundamental understanding of electrocatalytic processes at the nanoscale.

4.5. Surface Modification and Patterning

Most SECCM studies have focused on measuring local heterogeneities in the electrochemical response of various substrates. However, this technique can deliver species to a substrate in a controlled manner, thereby modifying the underlying substrate. Because the contact area between the meniscus and the surface defines the resolution of any modification and can be controlled by changing the probe size, it is possible to create or modify surface features with a resolution of < 100 nm, determined by the probe size.

Recent studies have used single-barreled pipettes, which have no positional feedback mechanism, to construct copper and platinum wires (87), conducting polymer structures (88, 89), and individual microcrystals (90). Theta pipettes have previously been used to construct patterns of biomolecules (53) and water droplets (54) on surfaces because they have a positioning system based on a modulated ion current, which is also the basis for positioning in SECCM. This robust feedback mechanism, coupled with the proven ability of SECCM to perform and monitor local electrochemical processes, is expected to help improve existing meniscus-based fabrication methods for the electrosynthesis of new structures from many different starting materials. We have demonstrated SECCM ‘reactive patterning’ to reveal the active sites for catechol oxidation at the basal surface of HOPG at the nanoscale (97).

4.6. Interfacial Ion-Transfer Processes

Although this review focuses mainly on SECCM as a technique to investigate the local electrochemical properties of electrically conducting substrates, the methodology is adaptable to the study of other systems. For example, the conductance current between the barrels can be tracked to follow processes that alter the conductivity of the droplet. The SECCM setup has been used to image ion uptake into a dental enamel sample (1), and static theta pipettes have been used in bulk solution to probe ion transfer (91). In the case of dental enamel, the localized uptake of ions by the sample causes a decrease in the conductance current that is mapped across the surface (1). Similarly, SECCM could readily be employed to study crystal growth or dissolution of ionic materials and minerals on a local scale. In such cases, SECCM would permit control over the flow of ions to the substrate by changing the bias between the barrel electrodes.

5. CONCLUSIONS AND PROSPECTS

In a relatively short time, SECCM has become a powerful new technique for electrochemistry and interfacial science, and it has a proven ability to quantitatively map interfacial charge transfer at the nanoscale. The technique is grounded on well-established electrochemical and general scanning probe microscopy principles and is underscored by a robust model for mass-transport and electric field calculations. This combination of experimental design and numerical modeling allows the ready interpretation of SECCM images and data in terms of key physicochemical processes, as illustrated by the examples discussed in this review.

SECCM is especially notable for providing a new understanding of the electrochemical behavior of carbon electrodes and allowing longstanding models for heterogeneous electron transfer to be rigorously tested and assessed. For example, SECCM imaging indicates that the basal surface of highly oriented pyrolytic graphite has considerable electroactivity. Similarly, we have elucidated the evolution of electrode kinetics from monolayer to multilayer arrangements of CVD grown graphene for the first time. pBDD electrodes have long been known to display spatially heterogeneous electron transfer rates, but the structural controls could not be established with conventional SECM imaging. In contrast, SECCM (combined with IC-SECM) has revealed detailed new information on local electron transfer and, furthermore, has allowed the visualization of complex (blocking) processes, which would have been difficult to achieve with SECM.

Given the great interest in nanostructured materials in electrochemistry, whose applications range from electrocatalysis to sensing, SECCM is a natural technique for selecting and visualizing the behavior of key components and relating this activity to structure at the nanoscale. The SECCM approach is particularly attractive because nanomaterials require little processing and encapsulation and can be studied in a (nearly) pristine state. SECCM has proven particularly powerful in elucidating and comparing the electrochemical activity of SWNTs: In studies of both two-dimensional networks and three-dimensional forests, it has demonstrated that the sidewall is highly active for outer-sphere redox couples and that sidewalls and closed ends have similar activity. Subtle differences in the morphology of nominally similar PtNPs cause significant variation in electroactivity; SECCM can target individual NPs within an ensemble or deliver individual NPs to an electrode surface for investigation. In all of these applications, the enhancement of information content through complementary microscopy and spectroscopy techniques on the same nanostructures has been crucial.

In the future, we expect SECCM to become a powerful method for nanofabrication and patterning under electrochemical control, particularly because our reaction imaging research has demonstrated that this technique can be applied to substrate materials ranging from electrical conductors to insulators. In this context, SECCM is expected to provide greater control and information content, given that it enables adaptive patterning “on the fly.”

Given the importance of interfacial ion-transfer processes in many areas and the difficulty of probing such processes on a local scale, SECCM could also have a significant impact in this area by functioning as a local conductivity cell to visualize ion uptake and release from surfaces and interfaces. Regarding the SECCM technique itself, it will be possible to further reduce the probe size, although doing so will probably require further development of the SECCM model to accommodate for possible substrate and pipette double-layer effects. There are also many options for enhancing the probes, such as building in additional channels for delivery, detection, and monitoring of interfacial processes.

DISCLOSURE STATEMENT

The authors are not aware of any affiliations, memberships, funding, or financial holdings that might be perceived as affecting the objectivity of this review.

ACKNOWLEDGMENTS

The authors are supported by the European Research Council under the European Community’s (EC’s) Seventh Framework Program (FP7/2007-2013)/ERC-2009-AdG2471143-QUANTIF. N.E. was supported by the Engineering and Physical Sciences Research Council (EPSRC) Collaborative Training Account scheme with the National Physical Laboratory, United Kingdom. A.G.G. and S.C.S.L. were further supported by EC (FP7/2007-2013) Marie Curie Intra-European Fellowships (projects 236885, “FUNSENS”, and 275450, “VISELCAT”) and by the EPSRC (EP/H023909/1). Further support was provided by the EPSRC for a studentship to K.M. (MOAC Doctoral Training Center). We acknowledge our coworkers at Warwick who have contributed greatly to the applications of SECCM. We are particularly grateful to Alex Colburn for his expert contributions.

LITERATURE CITED

1. Ebejer N, Schnippering M, Colburn AW, Edwards MA, Unwin PR. 2010. Localized high resolution electrochemistry and multifunctional imaging: scanning electrochemical cell microscopy. *Anal. Chem.* 82:9141--45
2. Bard AJ, Fan FRF, Kwak J, Lev O. 1989. Scanning electrochemical microscopy. Introduction and principles. *Anal. Chem.* 61:132--38
3. Kwak J, Bard AJ. 1989. Scanning electrochemical microscopy. Apparatus and two-dimensional scans of conductive and insulating substrates. *Anal. Chem.* 61:1794--99
4. Mirkin MV, Horrocks BR. 2000. Electroanalytical measurements using the scanning electrochemical microscope. *Anal. Chim. Acta* 406:119--46
5. Amemiya S, Bard AJ, Fan FRF, Mirkin MV, Unwin PR. 2008. Scanning electrochemical microscopy. *Annu. Rev. Anal. Chem.* 1:95--131
6. Mirkin MV, Nogala W, Velmurugan J, Wang Y. 2011. Scanning electrochemical microscopy in the 21st century. Update 1: five years after. *Phys. Chem. Chem. Phys.* 13:21196--212
7. Wittstock G, Burchardt M, Pust SE, Shen Y, Zhao C. 2007. Scanning electrochemical microscopy for direct imaging of reaction rates. *Angew. Chem. Int. Ed.* 46:1584--617
8. Engstrom RC, Pharr CM. 1989. Scanning electrochemical microscopy. *Anal. Chem.* 61:A1099
9. Macpherson JV, Unwin PR. 2000. Combined scanning electrochemical--atomic force microscopy. *Anal. Chem.* 72:276--85
10. Barker AL, Gonsalves M, Macpherson JV, Slevin CJ, Unwin PR. 1999. Scanning electrochemical microscopy: beyond the solid/liquid interface. *Anal. Chim. Acta* 385:223--40
11. Edwards MA, Martin S, Whitworth AL, Macpherson JV, Unwin PR. 2006. Scanning electrochemical microscopy: principles and applications to biophysical systems. *Physiol. Meas.* 27:R63
12. Gardner CE, Macpherson JV. 2002. Atomic force microscopy probes go electrochemical. *Anal. Chem.* 74:576--84A
13. Kranz C, Wiedemair J. 2008. Scanning force microscopy based amperometric biosensors. *Anal. Bioanal. Chem.* 390:239--43
14. Zhu Y, Williams DE. 1997. Scanning electrochemical microscopic observation of a precursor state to pitting corrosion of stainless steel. *J. Electrochem. Soc.* 144:43--45L

15. Kucernak AR, Chowdhury PB, Wilde CP, Kelsall GH, Zhu YY, Williams DE. 2000. Scanning electrochemical microscopy of a fuel-cell electrocatalyst deposited onto highly oriented pyrolytic graphite. *Electrochim. Acta* 45:4483--91
16. Meier J, Friedrich KA, Stimming U. 2002. Novel method for the investigation of single nanoparticle reactivity. *Faraday Discuss.* 121:365--72
17. Treutler TH, Wittstock G. 2003. Combination of an electrochemical tunneling microscope (ECSTM) and a scanning electrochemical microscope (SECM): application for tip-induced modification of self-assembled monolayers. *Electrochim. Acta* 48:2923--32
18. Ammann E, Beuret C, Indermuhle PF, Kotz R, de Rooij NF, Siegenthaler H. 2001. Local pH-controlled reactivity investigations by thin-layer scanning tunnelling microscopy. *Electrochim. Acta* 47:327--34
19. Ludwig M, Kranz C, Schuhmann W, Gaub HE. 1995. Topography feedback mechanism for the scanning electrochemical microscope based on hydrodynamic forces between tip and sample. *Rev. Sci. Instrum.* 66:2857--60
20. Hengstenberg A, Kranz C, Schuhmann W. 2000. Facilitated tip-positioning and applications of non-electrode tips in scanning electrochemical microscopy using a shear force based constant-distance mode. *Chem. Eur. J.* 6:1547--54
21. McKelvey K, Edwards MA, Unwin PR. 2010. Intermittent contact--scanning electrochemical microscopy (IC-SECM): a new approach for tip positioning and simultaneous imaging of interfacial topography and activity. *Anal. Chem.* 82:6334--37
22. Takahashi Y, Shevchuk AI, Novak P, Zhang YJ, Ebejer N, et al. 2011. Multifunctional nanoprobe for nanoscale chemical imaging and localized chemical delivery at surfaces and interfaces. *Angew. Chem. Int. Ed.* 50:9638--42
23. Shen M, Ishimatsu R, Kim J, Amemiya S. 2012. Quantitative imaging of ion transport through single nanopores by high-resolution scanning electrochemical microscopy. *J. Am. Chem. Soc.* 134:9856--59
24. Kim J, Shen M, Nioradze N, Amemiya S. 2012. Stabilizing nanometer scale tip-to-substrate gaps in scanning electrochemical microscopy using an isothermal chamber for thermal drift suppression. *Anal. Chem.* 84:3489--92
25. Zhan D, Li X, Zhan W, Fan FRF, Bard AJ. 2007. Scanning electrochemical microscopy. 58. Application of a micropipet-supported ITIES tip to detect Ag^+ and study its effect on fibroblast cells. *Anal. Chem.* 79:5225--31

26. Laforge FO, Velmurugan J, Wang Y, Mirkin MV. 2009. Nanoscale imaging of surface topography and reactivity with the scanning electrochemical microscope. *Anal. Chem.* 81:3143--50
27. Yatziv Y, Turyan I, Mandler D. 2002. A new approach to micropatterning: application of potential-assisted ion transfer at the liquid-liquid interface for the local metal deposition. *J. Am. Chem. Soc.* 124:5618--19
28. Cortes-Salazar F, Momotenko D, Lesch A, Wittstock G, Girault HH. 2010. Soft microelectrode linear array for scanning electrochemical microscopy. *Anal. Chem.* 82:10037--44
29. Cortes-Salazar F, Traeuble M, Li F, Busnel J-M, Gassner A-L, et al. 2009. Soft stylus probes for scanning electrochemical microscopy. *Anal. Chem.* 81:6889--96
30. Cortes-Salazar F, Lesch A, Momotenko D, Busnel J-M, Wittstock G, Girault HH. 2010. Fountain pen for scanning electrochemical microscopy. *Anal. Methods* 2:817--23
31. Böhni H, Suter T, Schreyer A. 1995. Microtechniques and nanotechniques to study localized corrosion. *Electrochim. Acta* 40:1361--68
32. Suter T, Böhni H. 1997. A new microelectrochemical method to study pit initiation on stainless steels. *Electrochim. Acta* 42:3275--80
33. Eng L, Wirth E, Suter T, Böhni H. 1998. Non-contact feedback for scanning capillary microscopy. *Electrochim. Acta* 43:3029--33
34. Hassel AW, Lohrengel MM. 1997. The scanning droplet cell and its application to structured nanometer oxide films on aluminium. *Electrochim. Acta* 42:3327--33
35. Lohrengel MM, Moehring A, Pilaski M. 2001. Capillary-based droplet cells: limits and new aspects. *Electrochim. Acta* 47:137--41
36. Lohrengel MM, Moehring A, Pilaski M. 2000. Electrochemical surface analysis with the scanning droplet cell. *Fresenius J. Anal. Chem.* 367:334--39
37. Lohrengel MM, Rosenkranz C, Klüppel I, Moehring A, Bettermann H, et al. 2004. A new microcell or microreactor for material surface investigations at large current densities. *Electrochim. Acta* 49:2863--70
38. Klemm SO, Schauer J-C, Schuhmacher B, Hassel AW. 2011. High throughput electrochemical screening and dissolution monitoring of Mg-Zn material libraries. *Electrochim. Acta* 56:9627--36
39. Klemm SO, Schauer J-C, Schuhmacher B, Hassel AW. 2011. A microelectrochemical scanning flow cell with downstream analytics. *Electrochim. Acta* 56:4315--21

40. Klemm SO, Pust SE, Hassel AW, Huepkes J, Mayrhofer KJJ. 2012. Electrochemical texturing of Al-doped ZnO thin films for photovoltaic applications. *J. Solid State Electrochem.* 16:283--90
41. Williams CG, Edwards MA, Colley AL, Macpherson JV, Unwin PR. 2009. Scanning micropipet contact method for high-resolution imaging of electrode surface redox activity. *Anal. Chem.* 81:2486--95
42. Day TM, Unwin PR, Macpherson JV. 2006. Factors controlling the electrodeposition of metal nanoparticles on pristine single walled carbon nanotubes. *Nano Lett.* 7:51--57
43. Dudin PV, Snowden ME, Macpherson JV, Unwin PR. 2011. Electrochemistry at nanoscale electrodes: individual single-walled carbon nanotubes (SWNTs) and SWNT-templated metal nanowires. *ACS Nano* 5:10017--25
44. Hansma PK, Drake B, Marti O, Gould SAC, Prater CB. 1989. The scanning ion-conductance microscope. *Science* 243:641--43
45. Shevchuk AI, Gorelik J, Harding SE, Lab MJ, Klenerman D, Korchev YE. 2001. Simultaneous measurement of Ca^{2+} and cellular dynamics: combined scanning ion conductance and optical microscopy to study contracting cardiac myocytes. *Biophys. J.* 81:1759--64
46. Chen C-C, Zhou Y, Baker LA. 2012. Scanning ion conductance microscopy. *Annu. Rev. Anal. Chem.* 5:207--28
47. Novak P, Li C, Shevchuk AI, Stepanyan R, Caldwell M, et al. 2009. Nanoscale live-cell imaging using hopping probe ion conductance microscopy. *Nat. Methods* 6:279--81
48. Gorelik J, Gu Y, Spohr HA, Shevchuk AI, Lab MJ, et al. 2002. Ion channels in small cells and subcellular structures can be studied with a smart patch-clamp system. *Biophys. J.* 83:3296--303
49. Dutta AK, Korchev YE, Shevchuk AI, Hayashi S, Okada Y, Sabirov RZ. 2008. Spatial distribution of maxi-anion channel on cardiomyocytes detected by smart-patch technique. *Biophys. J.* 94:1646--55
50. Comstock DJ, Elam JW, Pellin MJ, Hersam MC. 2010. Integrated ultramicroelectrode-nanopipet probe for concurrent scanning electrochemical microscopy and scanning ion conductance microscopy. *Anal. Chem.* 82:1270--76
51. Takahashi Y, Shevchuk AI, Novak P, Murakami Y, Shiku H, et al. 2010. Simultaneous noncontact topography and electrochemical imaging by SECM/SICM featuring ion current feedback regulation. *J. Am. Chem. Soc.* 132:10118--26

52. Takahashi Y, Shevchuk AI, Novak P, Zhang Y, Ebejer N, et al. 2011. Multifunctional nanoprobe for nanoscale chemical imaging and localized chemical delivery at surfaces and interfaces. *Angew. Chem. Int. Ed.* 50:9638--42
53. Rodolfa KT, Bruckbauer A, Zhou DJ, Korchev YE, Klenerman D. 2005. Two-component graded deposition of biomolecules with a double-barreled nanopipette. *Angew. Chem. Int. Ed.* 44:6854--59
54. Rodolfa KT, Bruckbauer A, Zhou DJ, Shevchuk AI, Korchev YE, Klenerman D. 2006. Nanoscale pipetting for controlled chemistry in small arrayed water droplets using a double-barrel pipet. *Nano Lett.* 6:252--57
55. Snowden ME, Güell AG, Lai SCS, McKelvey K, Ebejer N, et al. 2012. Scanning electrochemical cell microscopy: theory and experiment for quantitative high resolution spatially resolved voltammetry and simultaneous ion-conductance measurements. *Anal. Chem.* 84:2483--91
56. Lai SCS, Patel AN, McKelvey K, Unwin PR. 2012. Definitive evidence for fast electron transfer at pristine basal plane graphite from high-resolution electrochemical imaging. *Angew. Chem. Int. Ed.* 51:5405--8
57. Shao YH, Mirkin MV. 1998. Voltammetry at micropipet electrodes. *Anal. Chem.* 70:3155--61
58. Güell AG, Ebejer N, Snowden ME, Macpherson JV, Unwin PR. 2012. Structural correlations in heterogeneous electron transfer at monolayer and multilayer graphene electrodes. *J. Am. Chem. Soc.* 134:7258--61
59. Güell AG, Ebejer N, Snowden ME, McKelvey K, Macpherson JV, Unwin PR. 2012. Quantitative nanoscale visualization of heterogeneous electron transfer rates in 2D carbon nanotube networks. *Proc. Natl. Acad. Sci. USA* 109:11487--92
60. Lai SCS, Dudin PV, Macpherson JV, Unwin PR. 2011. Visualizing zeptomole (electro)catalysis at single nanoparticles within an ensemble. *J. Am. Chem. Soc.* 133:10744--47
61. Patten HV, Lai SCS, Macpherson JV, Unwin PR. 2012. Active sites for outer-sphere, inner-sphere, and complex multistage electrochemical reactions at polycrystalline boron--doped diamond electrodes (pBDD) revealed with scanning electrochemical cell microscopy (SECCM). *Anal. Chem.* 84:5427--32
62. White HS, Bund A. 2008. Mechanism of electrostatic gating at conical glass nanopore electrodes. *Langmuir* 24:12062--67

63. Wang G, Zhang B, Wayment JR, Harris JM, White HS. 2006. Electrostatic-gated transport in chemically modified glass nanopore electrodes. *J. Am. Chem. Soc.* 128:7679--86
64. Momotenko D, Cortes-Salazar F, Josserand J, Liu SJ, Shao YH, Girault HH. 2011. Ion current rectification and rectification inversion in conical nanopores: a perm-selective view. *Phys. Chem. Chem. Phys.* 13:5430--40
65. Bartle KD, Myers P. 2001. Theory of capillary electrochromatography. *J. Chromatogr. A* 916:3--23
66. Haynes WM, ed. 2002. *Handbook of Chemistry and Physics*. Boca Raton: CRC. 92nd ed.
67. Bonaccorso F, Sun Z, Hasan T, Ferrari AC. 2010. Graphene photonics and optoelectronics. *Nat. Photonics* 4:611--22
68. Sun Y-P, Fu K, Lin Y, Huang W. 2002. Functionalized carbon nanotubes: properties and applications. *Acc. Chem. Res.* 35:1096--104
69. Pate BB, Spicer WE, Ohta T, Lindau I. 1980. Electronic structure of the diamond (111) 1×1 surface: valence-band structure, band bending, and band gap states. *J. Vacuum Sci. Technol.* 17:1087--93
70. Morozov SV, Novoselov KS, Katsnelson MI, Schedin F, Elias DC, et al. 2008. Giant intrinsic carrier mobilities in graphene and its bilayer. *Phys. Rev. Lett.* 100:016602
71. Bertoncello P, Edgeworth JP, Macpherson JV, Unwin PR. 2007. Trace level cyclic voltammetry facilitated by single-walled carbon nanotube network electrodes. *J. Am. Chem. Soc.* 129:10982--83
72. Güell AG, Meadows KE, Unwin PR, Macpherson JV. 2010. Trace voltammetric detection of serotonin at carbon electrodes: comparison of glassy carbon, boron doped diamond and carbon nanotube network electrodes. *Phys. Chem. Chem. Phys.* 12:10108--14
73. Heller I, Kong J, Heering HA, Williams KA, Lemay SG, Dekker C. 2004. Individual single-walled carbon nanotubes as nanoelectrodes for electrochemistry. *Nano Lett.* 5:137--42
74. Patten HV, Meadows KE, Hutton LA, Iacobini JG, Battistel D, et al. 2012. Electrochemical mapping reveals direct correlation between heterogeneous electron-transfer kinetics and local density of states in diamond electrodes. *Angew. Chem. Int. Ed.* 51:7002--6

75. Wilson NR, Clewes SL, Newton ME, Unwin PR, Macpherson JV. 2006. Impact of grain-dependent boron uptake on the electrochemical and electrical properties of polycrystalline boron doped diamond electrodes. *J. Phys. Chem. B* 110:5639--46
76. Holt KB, Bard AJ, Show Y, Swain GM. 2004. Scanning electrochemical microscopy and conductive probe atomic force microscopy studies of hydrogen-terminated boron-doped diamond electrodes with different doping levels. *J. Phys. Chem. B* 108:15117--27
77. Wang S, Swain GM. 2007. Spatially heterogeneous electrical and electrochemical properties of hydrogen-terminated boron-doped nanocrystalline diamond thin film deposited from an argon-rich CH₄/H₂/Ar/B₂H₆ source gas mixture. *J. Phys. Chem. C* 111:3986--95
78. Neufeld A, O'Mullane A. 2006. Effect of the mediator in feedback mode-based SECM interrogation of indium tin oxide and boron-doped diamond electrodes. *J. Solid State Electrochem.* 10:808--16
79. Miller TS, Ebejer N, Güell AG, Macpherson JV, Unwin PR. 2012. Electrochemistry at carbon nanotube forests: sidewalls and closed ends allow fast electron transfer. *Chem. Commun.* 48:7435--37
80. Sarada BV, Rao TN, Tryk DA, Fujishima A. 2000. Electrochemical oxidation of histamine and serotonin at highly boron-doped diamond electrodes. *Anal. Chem.* 72:1632--38
81. Wrona MZ, Dryhurst G. 1987. Oxidation chemistry of 5-hydroxytryptamine. 1. Mechanism and products formed at micromolar concentrations. *J. Org. Chem.* 52:2817--25
82. Wrona MZ, Dryhurst G. 1990. Oxidation chemistry of 5-hydroxytryptamine. Part II. Mechanisms and products formed at millimolar concentrations in acidic aqueous solution. *J. Electroanal. Chem. Interfacial Electrochem.* 278:249--67
83. Reina A, Jia X, Ho J, Nezich D, Son H, et al. 2008. Large-area, few-layer graphene films on arbitrary substrates by chemical vapor deposition. *Nano Lett.* 9:30--35
84. Ferrari AC, Meyer JC, Scardaci V, Casiraghi C, Lazzeri M, et al. 2006. Raman spectrum of graphene and graphene layers. *Phys. Rev. Lett.* 97:187401
85. McCreery RL. 2008. Advanced carbon electrode materials for molecular electrochemistry. *Chem. Rev.* 108:2646--87
86. Fan Y, Goldsmith BR, Collins PG. 2005. Identifying and counting point defects in carbon nanotubes. *Nat. Mater* 4:906--11

87. Hu J, Yu MF. 2010. Meniscus-confined three-dimensional electrodeposition for direct writing of wire bonds. *Science* 329:313--16
88. Laslau C, Williams DE, Kannan B, Travas-Sejdic J. 2011. Scanned pipette techniques for the highly localized electrochemical fabrication and characterization of conducting polymer thin films, microspots, microribbons, and nanowires. *Adv. Funct. Mater.* 21:4607--16
89. Kim JT, Seol SK, Pyo J, Lee JS, Je JH, Margaritondo G. 2011. Three-dimensional writing of conducting polymer nanowire arrays by meniscus-guided polymerization. *Adv. Mater.* 23:1968--70
90. Yang DZ, Han LH, Yang Y, Zhao LB, Zong C, et al. 2011. Solid-state redox solutions: microfabrication and electrochemistry. *Angew. Chem. Int. Ed.* 50:8679--82
91. Liu B, Shao YH, Mirkin MV. 2000. Dual-pipet techniques for probing ionic reactions. *Anal. Chem.* 72:510--19
92. Kleijn SEF, Lai SCS, Miller TS, Yanson AI, Koper MTM, Unwin PR. 2012. Landing and catalytic characterization of individual nanoparticles on electrode surfaces. *J. Am. Chem. Soc.* 134: 18558-18561
93. Xiao X, Bard AJ. 2007. Observing single nanoparticle collisions at an ultramicroelectrode by electrocatalytic amplification. *J. Am. Chem. Soc.* 129: 9610-9612
94. Bard AJ, Zhou H, Kwon SJ. 2010. Electrochemistry of single nanoparticles via electrocatalytic amplification. *Isr. J. Chem.* 50: 267-276
95. Rees NV, Zhou Y-G, Compton RG. 2012. Making contact: charge transfer during particle-electrode collisions. *RSC Adv.* 2: 379-384
96. Patel AN, Collignon MG, O'Connell MA, Hung WOY, McKelvey K, Macpherson JV, Unwin PR. 2012. A new view of electrochemistry at highly oriented pyrolytic graphite. *J. Am. Chem. Soc.* 134: 20117-20130.
97. Patel AN, McKelvey K, Unwin PR. 2012. Nanoscale electrochemical patterning reveals the active sites for catechol oxidation at graphite surfaces. *J. Am. Chem. Soc.* doi: 10.1021/ja3095894